

Production of cascade hypernuclei via the (K^-, K^+) reaction within a quark-meson coupling model

R. Shyam^{1,2}, K. Tsushima¹, A.W. Thomas¹

¹ *Centre for the Subatomic Structure of Matter (CSSM),*

School of Chemistry and Physics, University of Adelaide, SA 5005, Australia

² *Saha Institute of Nuclear Physics,*

1/AF Bidhan Nagar, Kolkata 700064, India

(Dated: June 3, 2019)

Abstract

We study the production of bound hypernuclei $^{12}_{\Xi^-}\text{Be}$ and $^{28}_{\Xi^-}\text{Mg}$ via the (K^-, K^+) reaction on ^{12}C and ^{28}Si targets, respectively, within a covariant effective Lagrangian model, employing Ξ bound state spinors derived from the latest quark-meson coupling model as well as Dirac single particle wave functions. The $K^+\Xi^-$ production vertex is described by excitation, propagation and decay of Λ and Σ resonance states in the initial collision of a K^- meson with a target proton in the incident channel. The parameters of the resonance vertices are fixed by describing the available data on total and differential cross sections for the $p(K^-, K^+)\Xi^-$ reaction. We find that both the elementary and hypernuclear production cross sections are dominated by the contributions from the $\Lambda(1520)$ intermediate resonant state. The 0° differential cross sections for the formation of simple s-state Ξ^- particle-hole states peak at a beam momentum around 1.0 GeV/c, with a value in excess of $1 \mu\text{b}$.

PACS numbers: 25.80.Nv, 24.85.+p, 13.75.Jz

The study of the double strangeness (S) hypernuclei is of decisive importance for revealing the entire picture of strong interactions among octet baryons. The binding energies and widths of the Ξ hypernuclear states are expected to determine the strength of the ΞN and $\Xi N \rightarrow \Lambda\Lambda$ interactions, respectively. This basic information is key to testing the quark exchange aspect of the strong interaction, since long range pion exchange plays essentially a very minor role in the $S = -2$ sector. This input is also vital for understanding the multi-strange hadronic or quark matter. Since strange quarks are negatively charged they are preferred in charge neutral dense matter. Thus these studies are of crucial value for investigating the role of strangeness in the equation of state at high density, as probed in the cores of neutron stars [1, 2] and in high energy heavy ion collisions at relativistic heavy ion colliders (RHIC) at Brookhaven National laboratory [3], CERN [4] and FAIR facility at GSI [5].

The (K^-, K^+) reaction leads to the transfer of two units of both charge and strangeness to the target nucleus. Thus this reaction is one of the most promising ways of studying the $S = -2$ systems such as Ξ hypernuclei and a dibaryonic resonance (H), which is a near stable six-quark state with spin parity of 0^+ and isospin 0 [6–8]. Several ways have been discussed to approach these systems in the past. These range from the atomic capture of Ξ^- created in free space by the (K^-, K^+) reaction [9] to the (K^-, K^+) reaction on nuclear targets [10–13].

As far as Ξ hypernuclei are concerned, there are some hints of their existence from emulsion events [14]. However, no Ξ bound state was unambiguously observed in the few experiments performed involving the (K^-, K^+) reaction on a ^{12}C target [12, 13] because of the limited statistics and detector resolution. However, in the near future experiments will be performed at the JPARC facility in Japan to observe the bound states of Ξ hypernuclei via the (K^-, K^+) reaction with the best energy resolution of a few MeV and with large statistics by using the newly constructed high-resolution spectrometers [15]. The first series of experiments will be performed on a ^{12}C target. These measurements are of great significance because convincing evidence for the Ξ single-particle bound states would yield vital information on Ξ single particle potential and the effective ΞN interaction. Already, the analysis of the scarce emulsion [16] and spectrometer data [12, 13] have led to Ξ -nuclear potentials with depths that differ by about 10 MeV from each other.

The (K^-, K^+) reaction implants a Ξ hyperon in the nucleus through the elementary

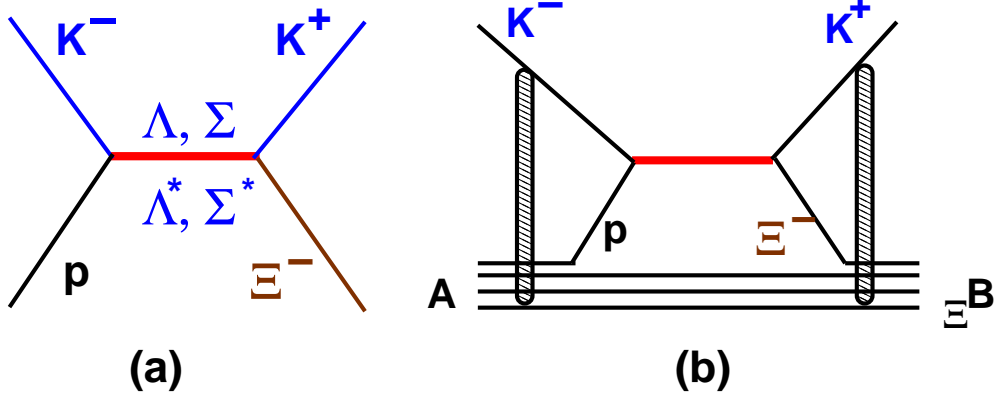


FIG. 1: (color online) Graphical representation of our model to describe $p(K^-, K^+)\Xi^-$ (Fig. 1a) and $A(K^-, K^+)\Xi^- B$ reactions (Fig. 2b). In the latter case the shaded area depicts the optical model interactions in the incoming and outgoing channels.

process $p(K^-, K^+)\Xi^-$. The cross sections for the elementary reaction were measured in the 1960s and early 1970s using hydrogen bubble chambers [17, 18]. The total-cross-section data from these measurements are tabulated in Ref. [19]. In a recent study [20], this reaction was investigated within a single-channel effective Lagrangian model where contributions were included from the s -channel [see, Fig. 1(a)] and u -channel diagrams which have as intermediate states Λ and Σ hyperons together with eight of their three- and four-star resonances with masses up to 2.0 GeV [$\Lambda(1405)$, $\Lambda(1520)$, $\Lambda(1670)$, $\Lambda(1810)$, $\Lambda(1890)$, $\Sigma(1385)$, $\Sigma(1670)$ and $\Sigma(1750)$, which are represented by Λ^* and Σ^* in Fig. 1a]. This reaction is a clean example of a process in which baryon exchange plays the dominant role and the t -channel meson exchanges are absent, as no meson with $S = +2$ is known to exist. An important observation of that study is that the total cross section of the $p(K^-, K^+)\Xi^-$ reaction is dominated by the contributions from the $\Lambda(1520)$ (with $L_{IJ} = D_{03}$) resonance intermediate state through both s - and u -channel terms. The region for beam momentum (p_{K^-}) below 2.0 GeV/c was shown to get most contributions from the s -channel graphs - the u -channel terms are dominant only in the region $p_{K^-} > 2.5$ GeV.

Almost all of the previous theoretical investigations of cascade hypernuclear production via (K^-, K^+) reaction on target nuclei [16, 21–24] have used the framework of an impulse approximation where the hyperon production dynamics is separated from that of the relative motion in the entrance and outgoing channels. Thus, the hypernuclear production cross section is expressed as a product of the cross section of the elementary cascade production

reaction and a term that accounts for the dynamics of the relative motion. None of these models has attempted to calculate the cross sections of the elementary reaction - they have been extracted from the sparse experimental data. Therefore, the results of these calculations carry over the ambiguities that are involved in the experimental values of the differential cross sections for the elementary reactions.

In this paper, we investigate the production of cascade hypernuclei via the (K^-, K^+) reaction on nuclear targets within an effective Lagrangian model [25–27], which is similar to that used in Ref. [20] to study the elementary production reaction, $p(K^-, K^+)\Xi^-$. We consider only the s -channel production diagrams (see Fig. 1b) as we are interested in the region where p_{K^-} lies below 2 GeV/ c . The model retains the full field theoretic structure of the interaction vertices and treats baryons as Dirac particles. The initial state interaction of the incoming K^- with a bound target proton leads to excitation of intermediate Λ and Σ resonant states, which propagate and subsequently decay into a Ξ^- hyperon that gets captured into one of the nuclear orbits, while the other decay product, the K^+ goes out. In Ref. [20], it was shown that six intermediate resonant states, Λ , $\Lambda(1405)$, $\Lambda(1520)$, $\Lambda(1810)$, Σ , and $\Sigma(1385)$, make the most significant contributions to the cross sections of the elementary process. Therefore, in our present study the amplitudes corresponding to these six resonant states have been considered.

The Ξ^- bound state spinors have been calculated in the quark-meson coupling (QMC) model as well as in a phenomenological model where they are obtained by solving the Dirac equation with scalar and vector fields having a Woods-Saxon radial form. In the latter case, with a set of radius and diffuseness parameters, the depths of these fields are searched to reproduce the binding energy (BE) of a given state. Since the experimental values of the BEs for the Ξ^- bound states are as yet unknown, we have adopted the corresponding QMC model predictions (as shown in table 1) in our search procedure for these states. It should be noted that the depths of the potential fields in the phenomenological model are dependent on the adopted radius and diffuseness parameters but there is no certain way of fixing them. Furthermore, the scalar and vector fields are assumed to have the same geometry. With these constraints, we show in Table 1 the resulting parameters associated with the scalar and vector fields of the phenomenological model for Ξ^- bound and proton hole states for the two target nuclei. In Table 1 the QMC predictions for the BE of the proton hole states are also shown. However, in the search procedure for these states the experimental values

TABLE I: Dirac single particle potential parameters for the Ξ^- bound states and proton hole states. In each case radius and diffuseness parameters were $r = 0.983$ fm, and $a = 0.606$ fm, respectively. The binding energies (BEs) of the Ξ^- states are the predictions of the QMC model. The QMC BEs for the proton hole states are also shown together with the corresponding experimental values (given within the brackets).

| State | BE (MeV) | V_v (MeV) | V_s (MeV) |
|-------------------------------------|----------------|----------------|----------------|
| $^{12}_{\Xi^-}\text{-Be}(1s_{1/2})$ | 5.681 | 104.840 | -141.910 |
| $^{28}_{\Xi^-}\text{-Mg}(1s_{1/2})$ | 11.376 | 124.674 | -153.881 |
| $^{28}_{\Xi^-}\text{-Mg}(1p_{3/2})$ | 5.490 | 167.124 | -206.326 |
| $^{12}\text{C}(1p_{3/2})$ | 14.329(15.957) | 382.598 | -472.343 |
| $^{28}\text{Si}(1d_{5/2})$ | 10.071(11.585) | 378.421 | -467.186 |

of the BEs (given within the brackets) have been used.

The use of bound state spinors calculated within the quark-meson coupling (QMC) model provides an opportunity to investigate the role of the quark degrees of freedom in the cascade hypernuclear production, which has not been done in previous studies of this system. Since the cascade hypernuclear production involves large momentum transfers (350 MeV/c - 600 MeV/c) to the target nucleus, it is a good case for examining such short distance effects. In the QMC model [28], quarks within the non-overlapping nucleon bags (modeled using the MIT bag), interact self consistently with isoscalar-scalar (σ) and isoscalar-vector (ω) mesons in the mean field approximation. The explicit treatment of the nucleon internal structure represents an important departure from quantum hadrodynamics (QHD) model [29]. The self-consistent response of the bound quarks to the mean σ field leads to a new saturation mechanism for nuclear matter [28]. The QMC model has been used to study the properties of finite nuclei [30], the binding of ω , η , η' and D nuclei [31–33] and also the effect of the medium on K^\pm and J/Ψ production [34].

The most recent development of the quark-meson coupling model is the inclusion of the self-consistent effect of the mean scalar field on the familiar one-gluon exchange hyperfine interaction that in free space leads to the $N - \Delta$ and $\Sigma - \Lambda$ mass splitting [35]. With this [36] the QMC model has been able to explain the properties of Λ hypernuclei for the s -states

rather well, while the p - and d -states tend to underbind. It also leads to a very natural explanation of the small spin-orbit force in Λ -nucleus interaction. In this exploratory work, the bound Ξ spinors are generated from this version of the QMC model and are used to calculate the cross sections of the $^{12}\text{C}(K^-, K^+)_{\Xi}^{12}\text{-Be}$ and $^{28}\text{Si}(K^-, K^+)_{\Xi}^{28}\text{-Mg}$ reactions.

To calculate the bound state spinors, we have used the latest version of the QMC model. In this version, while the quality of results for Λ and Ξ is comparable that of the earlier QMC results [32], no bound states for the Σ states [36] are found. The latter is in agreement with the experimental observations. This is facilitated by the extra repulsion associated with the increased one-gluon-exchange hyperfine interaction in medium. We refer to Ref. [36] for more details of this new version of the QMC.

In order to calculate the properties of finite hypernuclei, we construct a simple, relativistic shell model, with the nucleon core calculated in a combination of self-consistent scalar and vector mean fields. The Lagrangian density for a hypernuclear system in the QMC model is written as a sum of two terms, $\mathcal{L}_{QMC}^{HY} = \mathcal{L}_{QMC} + \mathcal{L}_{QMC}^Y$, where [31],

$$\begin{aligned} \mathcal{L}_{QMC} = & \bar{\psi}_N(\mathbf{r})[i\boldsymbol{\gamma} \cdot \boldsymbol{\partial} - M_N(\sigma) - (g_\omega\omega(\mathbf{r}) \\ & + g_\rho \frac{\tau_3^N}{2} b(\mathbf{r}) + \frac{e}{2}(1 + \tau_3^N)A(\mathbf{r}))\gamma_0]\psi_N(\mathbf{r}) \\ & - \frac{1}{2}[(\nabla\sigma(\mathbf{r}))^2 + m_\sigma^2\sigma(\mathbf{r})^2] \\ & + \frac{1}{2}[(\nabla\omega(\mathbf{r}))^2 + m_\omega^2\omega(\mathbf{r})^2] \\ & + \frac{1}{2}[(\nabla b(\mathbf{r}))^2 + m_\rho^2 b(\mathbf{r})^2] + \frac{1}{2}(\nabla A(\mathbf{r}))^2, \end{aligned} \quad (1)$$

and

$$\begin{aligned} \mathcal{L}_{QMC}^Y = & \sum_{Y=\Lambda, \Sigma, \Xi} \bar{\psi}_Y(\mathbf{r})[i\boldsymbol{\gamma} \cdot \boldsymbol{\partial} - M_Y(\sigma) - (g_\omega^Y\omega(\mathbf{r}) \\ & + g_\rho^Y I_3^Y b(\mathbf{r}) + eQ_Y A(\mathbf{r}))\gamma_0]\psi_Y(\mathbf{r}), \end{aligned} \quad (2)$$

where $\psi_N(\mathbf{r})$, $\psi_Y(\mathbf{r})$, $b(\mathbf{r})$ and $\omega(r)$ are, respectively, the nucleon, hyperon, the ρ meson and the ω meson fields, while m_σ , m_ω and m_ρ are the masses of the σ , ω and ρ mesons. The $A(r)$ is Coulomb field. g_ω and g_ρ are the ω -N and ρ -N coupling constants which are related to the corresponding (u,d)-quark- ω , g_ω^q , and (u, d) quark- ρ , g_ρ^q , coupling constants as $g_\omega = 3g_\omega^q$ and $g_\rho = g_\rho^q$. I_3^Y and Q_Y are the third component of the hyperon isospin operator and its electric charge in units of the proton charge, e , respectively.

The following set of equations of motion are obtained for the hypernuclear system from the Lagrangian density Eqs. (1)-(2):

$$[i\gamma \cdot \partial - M_N(\sigma) - (g_\omega \omega(\mathbf{r}) + g_\rho \frac{\tau_3^N}{2} b(\mathbf{r}) + \frac{e}{2}(1 + \tau_3^N)A(\mathbf{r}))\gamma_0]\psi_N(\mathbf{r}) = 0, \quad (3)$$

$$[i\gamma \cdot \partial - M_Y(\sigma) - (g_\omega^Y \omega(\mathbf{r}) + g_\rho^Y I_3^Y b(\mathbf{r}) + eQ_Y A(\mathbf{r}))\gamma_0]\psi_Y(\mathbf{r}) = 0, \quad (4)$$

$$(-\nabla_r^2 + m_\sigma^2)\sigma(\mathbf{r}) = g_\sigma C_N(\sigma)\rho_s(\mathbf{r}) + g_\sigma^Y C_Y(\sigma)\rho_s^Y(\mathbf{r}), \quad (5)$$

$$(-\nabla_r^2 + m_\omega^2)\omega(\mathbf{r}) = g_\omega \rho_B(\mathbf{r}) + g_\omega^Y \rho_B^Y(\mathbf{r}), \quad (6)$$

$$(-\nabla_r^2 + m_\rho^2)b(\mathbf{r}) = \frac{g_\rho}{2}\rho_3(\mathbf{r}) + g_\rho^Y I_3^Y \rho_B^Y(\mathbf{r}), \quad (7)$$

$$(-\nabla_r^2)A(\mathbf{r}) = e\rho_p(\mathbf{r}) + eQ_Y \rho_B^Y(\mathbf{r}), \quad (8)$$

where, $\rho_s(\mathbf{r})$ ($\rho_s^Y(\mathbf{r})$), $\rho_B(\mathbf{r})$ ($\rho_B^Y(\mathbf{r})$), $\rho_3(\mathbf{r})$ and $\rho_p(\mathbf{r})$ are the scalar, baryon, third component of isovector, and proton densities at the position \mathbf{r} in the hypernucleus [31]. On the right hand side of Eq. (5), a new and characteristic feature of QMC appears, arising from the internal structure of the nucleon and hyperon, namely, $g_\sigma C_N(\sigma) = -\frac{\partial M_N(\sigma)}{\partial \sigma}$ and $g_\sigma^Y C_Y(\sigma) = -\frac{\partial M_Y(\sigma)}{\partial \sigma}$ where $g_\sigma \equiv g_\sigma(\sigma = 0)$ and $g_\sigma^Y \equiv g_\sigma^Y(\sigma = 0)$. We use the nucleon and hyperon masses as parameterized in Ref. [36]. The scalar and vector fields as well as the spinors for hyperons and nucleons, can be obtained by solving these coupled equations self-consistently.

In Figs. 2(a) and Figs 2(c), we compare the scalar and vector fields as calculated within the QMC model with those of the phenomenological model for $1s_{1/2} \Xi^-$ states of $^{12}_{\Xi^-}\text{Be}$ and $^{28}_{\Xi^-}\text{Mg}$ hypernuclei, respectively. It may be recalled that in the QMC model the scalar and vector fields are generated by the couplings of the σ and ω mesons to the quarks. Because of the different masses of these mesons and their couplings to the quark fields the scalar and vector fields acquire a different radial dependence. In contrast, the two fields have the same

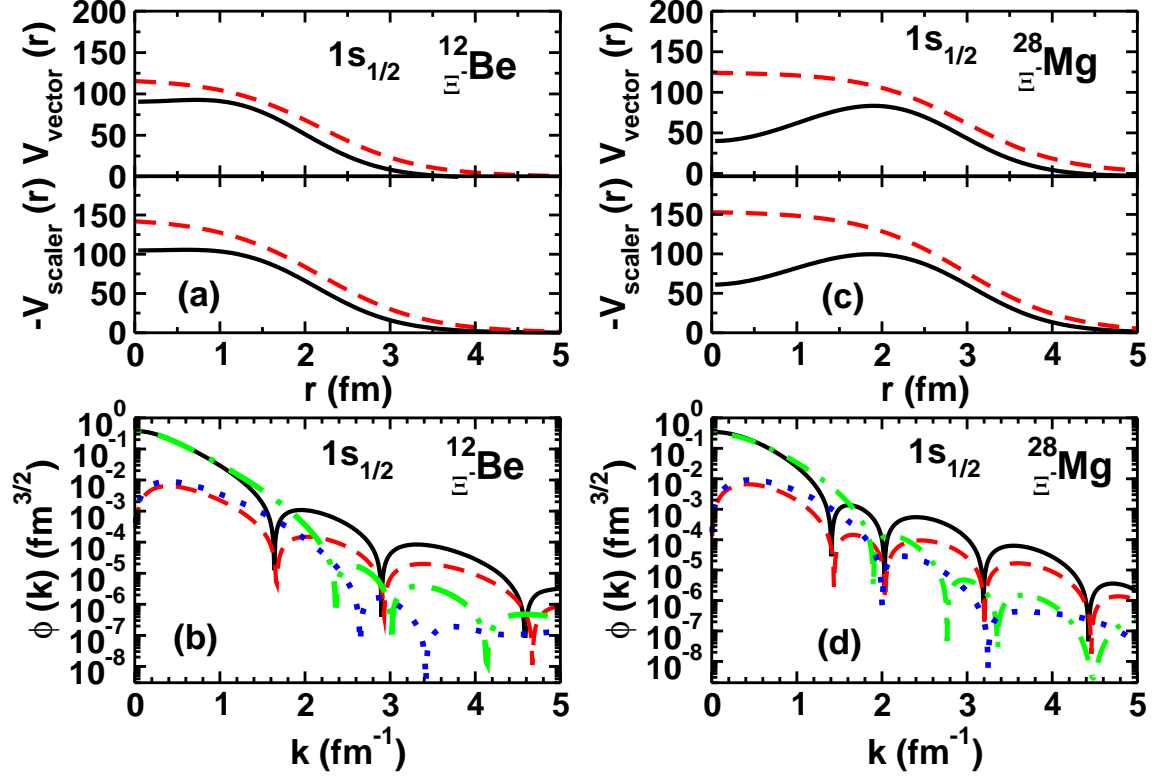


FIG. 2: (color online) [(a)] Vector and scalar potential fields for $1s_{1/2}$ Ξ state in $^{12}_{\Xi}\text{-Be}$. The QMC model and Dirac single particle results are shown by solid and dashed lines, respectively. [(b)] Moduli of the upper ($|f|$) and lower ($|g|$) components of the $1s_{1/2}$ Ξ orbits in $^{12}_{\Xi}\text{-B}$ hypernucleus in momentum space. $|f|$ and $|g|$ of the QMC model are shown by the solid and dashed lines, respectively while those of the phenomenological model by the dashed-dotted and dotted lines, respectively. [(c)] and [d] represent the same for $^{28}_{\Xi}\text{-Mg}$ hypernucleus.

radial shapes in the phenomenological model. We notice that in general, the QMC scalar and vector fields are smaller in magnitude than those of the phenomenological model in the entire r -region. One interesting point to note is that for the heavier hypernucleus, both scalar and vector QMC fields have their maxima away from the point $r = 0$, in contrast to the phenomenological fields. In the mean field models of the finite nuclei the proton densities are somewhat pushed out as compared to those of the neutron, because of Coulomb repulsion. This causes the Ξ^- potential to peak outside the center of the nucleus. This is a consequence of the self consistent procedure. In the case of a chargeless hyperon (e.g. Λ) such effects are not observed.

In Figs. 2(b) and 2(d) the moduli of the upper and lower components of $1s_{1/2}$ Ξ^- momen-

tum space QMC (solid and dashed line) and phenomenological (dashed-dotted and dotted) spinors are shown for the $^{12}_{\Xi}$ -Be and $^{28}_{\Xi}$ -Mg hypernuclei, respectively. It is seen that the spinors of the two models are similar to each other for momenta (k) up to 2.0 fm^{-1} . Beyond this region, however, they start having differences. The position of minima in the phenomenological model spinors is shifted to higher values of k and their magnitudes are smaller than those of the QMC model. We further note that only for k values below 1.5 fm^{-1} , are the magnitudes of the lower components, $|g(k)|$, substantially smaller than those of the upper components. In the region of k pertinent to the cascade hypernuclear production, $|g(k)|$ may not be negligible. Thus the relativistic effects resulting from the small component of bound states spinors could be large for the hypernuclear production reactions on nuclei (see also the discussions presented in Ref. [37]).

The effective Lagrangians for the resonance-kaon-baryon vertices for spin- $\frac{1}{2}$ and spin- $\frac{3}{2}$ resonances are taken as

$$\mathcal{L}_{KBR_{1/2}} = -g_{KBR_{1/2}} \bar{\psi}_{R_{1/2}} [\chi i\Gamma \varphi_K + \frac{(1-\chi)}{M} \Gamma \gamma_\mu (\partial^\mu \varphi_K)] \psi_B, \quad (9)$$

$$\mathcal{L}_{KBR_{3/2}} = \frac{g_{KBR_{3/2}}}{m_K} \bar{\psi}_{R_{3/2}}^\mu \partial_\mu \phi_K \psi_B + \text{h. c.}, \quad (10)$$

with $M = (m_R \pm m_B)$, where the upper sign corresponds to an even-parity and the lower sign to an odd-parity resonance, and B represents either a nucleon or a Ξ hyperon. The operator Γ is γ_5 (1) for an even- (odd-) parity resonance. The parameter χ controls the admixture of pseudoscalar and pseudovector components. The value of this parameter is taken to be 0.5 for the Λ^* and Σ^* states, but zero for Λ and Σ states, implying pure pseudovector couplings for the corresponding vertices in agreement with Refs. [26, 38]. It may be noted that the Lagrangian for spin- $\frac{3}{2}$ as given by Eq. (10) corresponds to that of a pure Rarita-Swinger form which has been used in all previous calculations of the hypernuclear production reactions within a similar effective Lagrangian model [25–27]. We have used, at various vertices, form factors which is similar to that employed in Ref. [20] with the same value of the cutoff parameter.

The parameters of the resonance vertices were fixed in Ref. [20] by describing the total cross section data on elementary reactions $p(K^-, K^+) \Xi^-$ and $p(K^-, K^0) \Xi^0$, where the form of the spin- $\frac{3}{2}$ interaction vertex was somewhat different form that given Eq. (10). In this paper, therefore, we recalculate the cross sections of the elementary reaction using the spin- $\frac{3}{2}$ Lagrangian given by Eq. (10). Apart from the total cross sections, we also describe the

TABLE II: Λ and Σ resonance intermediate states included in the calculation.

| Intermediate state (R) | L_{IJ} | M (GeV) | $Width$ (GeV) | g_{KRN} | $g_{KR\Xi}$ |
|-------------------------------|----------|--------------|------------------|-----------|-------------|
| Λ | | 1.116 | 0.0 | -16.750 | 10.132 |
| Σ | | 1.189 | 0.0 | 5.580 | -13.50 |
| $\Sigma(1385)$ | P_{13} | 1.383 | 0.036 | -8.22 | -8.220 |
| $\Lambda(1405)$ | S_{01} | 1.406 | 0.050 | 1.585 | -0.956 |
| $\Lambda(1520)$ | D_{03} | 1.520 | 0.016 | 27.46 | -16.610 |
| $\Lambda(1810)$ | P_{01} | 1.810 | 0.150 | 2.800 | 2.800 |

differential cross sections of the $p(K^-, K^+)\Xi^-$ reaction which was not done in Ref. [20]. The values of the vertex parameters were taken to be the same as those determined in Ref. [20] except for the vertices involving the $\Sigma(1385)$ resonance, where the coupling constants (CCs) have been slightly increased in order to better describe the differential cross section data (see Table 2).

In Figs. 3a, we show comparisons of our calculations with the data for the total cross section of the $p(K^-, K^+)\Xi^-$ reaction for K^- beam momenta (p_{K^-}) below 3.5 GeV/c, because the resonance picture is not suitable at momenta higher than this. It is clear that our model is able to describe well the beam momentum dependence of the total cross section data of the elementary reactions within statistical errors. The arrow in Fig. 3a shows the position of the threshold beam momentum for this reaction which is about 1.0 GeV. The measured total cross section peaks in the region of 1.35-1.4 GeV/c which is well described by our model. We further note that the cross sections for $p_{K^-} < 2.0$ GeV/c are dominated by the s -channel contributions.

In Fig. 3b we compare our calculations with the differential cross section data of the $p(K^-, K^+)\Xi^-$ reaction for p_{K^-} values of 1.7 GeV/c and 2.1 GeV/c. These data were read from the corresponding figures given in Ref. [18]. Both calculated and experimental differential cross sections are normalized to the same total cross section. We see that our calculations describe the general trends of the angular distribution data well in the entire angular region for both the beam momenta. Nevertheless, a slight overestimate of the data is noted at the forward angles. There is a need to remeasure these differential cross sections

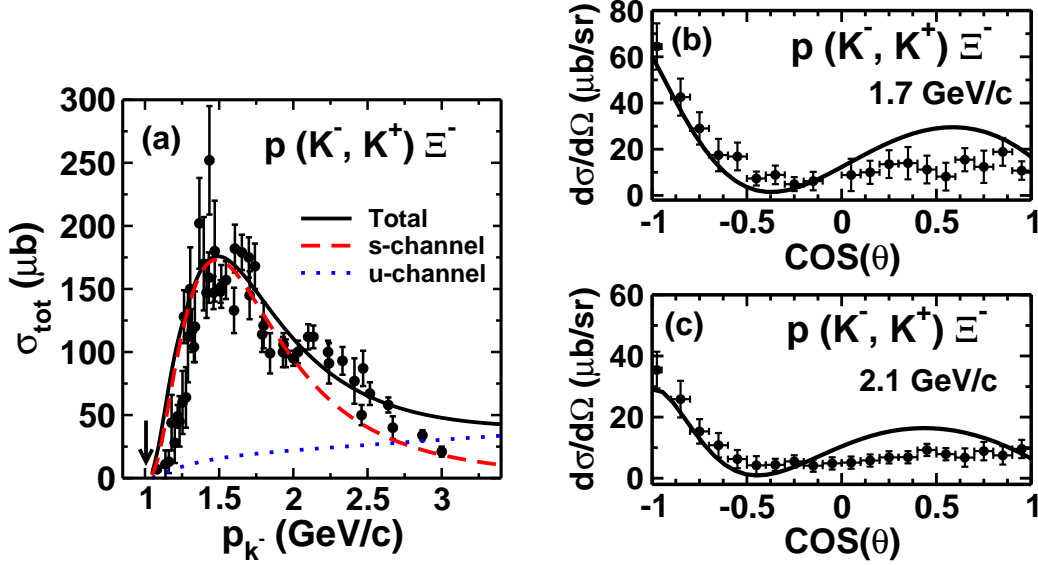


FIG. 3: (color online) (a) Comparison of the calculated total cross section for the $p(K^-, K^+)\Xi^-$ reaction as a function of incident K^- momentum with the corresponding experimental data. Also shown are the individual contributions of s - and u -channel diagrams to the total cross section. The arrow indicates the position of the threshold for this reaction. (b) and (c) Differential cross sections for the same reaction for K^- beam momenta of $1.7 \text{ GeV}/c$ and $2.1 \text{ GeV}/c$, respectively.

at the JPARC facility to confirm and refine the old bubble chamber data of Ref. [18].

The two interaction vertices of Fig. 1 are connected by a resonance propagator. For the spin-1/2 and spin-3/2 resonances the propagators are given by

$$\mathcal{D}_{R_{1/2}} = \frac{i(\gamma_\mu p^\mu + m_{R_{1/2}})}{p^2 - (m_{R_{1/2}} - i\Gamma_{R_{1/2}}/2)^2}, \quad (11)$$

and

$$\mathcal{D}_{R_{3/2}}^{\mu\nu} = -\frac{i(\gamma_\lambda p^\lambda + m_{R_{3/2}})}{p^2 - (m_{R_{3/2}} - i\Gamma_{R_{3/2}}/2)^2} P^{\mu\nu}, \quad (12)$$

respectively. In Eq. (12) we have defined

$$P^{\mu\nu} = g^{\mu\nu} - \frac{1}{3}\gamma^\mu\gamma^\nu - \frac{2}{3m_{R_{3/2}}^2}p^\mu p^\nu + \frac{1}{3m_{R_{3/2}}} (p^\mu\gamma^\nu - p^\nu\gamma^\mu). \quad (13)$$

In Eqs. (11) and (12), $\Gamma_{R_{1/2}}$ and $\Gamma_{R_{3/2}}$ define the total widths of the corresponding resonances. We have ignored any medium modification of the resonance widths while calculating the amplitudes of the hypernuclear production as information about them is scarce and uncertain.

After having established the vertices and corresponding coupling constants as well as the form of the propagators, the amplitudes of the graphs of the type shown in Fig. 1 can be written by following the well known Feynman rules. We have employed pure single-particle-single-hole (Ξp^{-1}) wave functions to describe the nuclear structure part, ignoring any configuration mixing effects. The nuclear structure part is treated exactly in the same way as described in Ref. [26]. The amplitude involves the momentum space four component (spin space) spinors (ψ) which represent the wave functions of the bound states of nucleon and hyperon. For the proton hole and Ξ^- states, spinors generated within the QMC and the phenomenological models were used in the respective calculations. We have used a plane wave approximation to describe the relative motion of kaons in the incoming and outgoing channels. However, the distortion effects are partially accounted for by introducing reduction factors to the cross sections as described in Ref. [22]. Since our calculations are carried out all along in momentum space, they include all the nonlocalities in the production amplitudes that arise from the resonance propagators.

We have chosen the reactions $^{12}\text{C}(K^-, K^+)_{\Xi}^{12}\text{-Be}$ and $^{28}\text{Si}(K^-, K^+)_{\Xi}^{28}\text{-Mg}$ for the first application of our model. The reaction on the ^{12}C target is billed as the "day one" experiment at the JPARC facility. The thresholds for these reactions are about 0.761 GeV/c and 0.750 GeV/c, respectively and the momentum transfers involved at 0° , vary between 1.8 - 2.9 fm^{-1} . The initial states in both the cases are doubly closed systems. The QMC model predicts only one bound state for the $^{12}_{\Xi}\text{-Be}$ hypernucleus with the Ξ^- hyperon being in a $1s_{1/2}$ state with a binding energy as shown in Table 1. This can populate 1^- and 2^- states of the hypernucleus corresponding to the particle-hole configuration $[(1p_{3/2})_p^{-1}, (1s_{1/2})_{\Xi-}]$. For the $^{28}_{\Xi}\text{-Mg}$ case however, three distinct bound Ξ^- states with configurations $1s_{1/2}$, $1p_{3/2}$ and $1p_{1/2}$ have been predicted. The binding energies of first two states, which are chosen in the present calculations are also shown in Table 2. The $1p_{1/2}$ state has a binding energy of 5.4902 MeV. The hypernuclear states populated for $^{28}_{\Xi}\text{-Mg}$ are 2^+ , 3^+ and 1^- , 2^- , 3^- , 4^- corresponding to the configurations $[(1d_{5/2})_p^{-1}, (1s_{1/2})_{\Xi-}]$ and $[(1d_{5/2})_p^{-1}, (1p_{3/2})_{\Xi-}]$, respectively.

In Fig. 4a, we show the beam momentum dependence of the 0° differential cross sections obtained by using Ξ^- bound state spinors within the QMC as well as the phenomenological model for the reactions $^{12}\text{C}(K^-, K^+)_{\Xi}^{12}\text{-Be}$ and $^{28}\text{Si}(K^-, K^+)_{\Xi}^{28}\text{-Mg}$. The configurations of the final hypernuclear states are as described in the figure caption. The distortion factor, which primarily describes the absorption of the incoming K^- , represents a reduction in the

cross sections by factors of 2.8 and 5.0 for ^{12}C and ^{28}Si targets, respectively as suggested in Ref. [22]. In each case results are for populating the hypernuclear state with maximum spin of natural parity. We see that the QMC model cross sections are larger than those obtained by using the phenomenological model by about 10-20% in all the cases. This reflects the fact that in the region of momentum transfers relevant to these reactions both the upper and the lower components of the QMC spinors are higher in magnitude than the corresponding phenomenological ones.

An important observation in Fig. 4a is that for both the hypernuclear production reactions, the cross sections peak at p_{K^-} around 1.0 GeV/c, which is about 0.25-0.26 GeV/c above the production thresholds of the two reactions. Interestingly, it is not too different from the case of the elementary Ξ^- production reaction where the peak of the total cross section occurs at about 0.35-0.40 GeV/c above the corresponding production threshold (see Fig. 3a). Furthermore, the magnitudes of the cross sections near the peak position are in excess of $1 \mu\text{b}$. It is important in this context to note that the magnitude of our cross section for a ^{12}C target at a beam momentum of 1.6 GeV/c is similar to that obtained in Ref. [22] within an impulse approximation model. Moreover, our cross sections at 1.8 GeV/c also are very close those of Ref. [16] for both the targets. However, we fail to corroborate the results of Ref. [16] where cross sections were shown to peak for p_{K^-} around 1.8 GeV/c. It is quite probable that the distortion effects are dependent on the beam momenta and may be relatively stronger at lower values of p_{K^-} . Nevertheless, this is not likely to lead to such a large shift in the peak position. In any case, this effect was not considered in Ref. [16]. There may be a need to re-examine the beam momentum dependence of the zero degree differential cross section used in the calculations of that reference.

In Fig 4b, we note that the contribution from the $\Lambda(1520)$ intermediate state dominates the total cross sections over the entire regime of p_{K^-} values. This is similar to that noted in the case of the elementary Ξ^- production reaction. The $\Lambda(1405)$, and $\Sigma(1385)$ states make noticeable contributions only for p_{K^-} very close to the production threshold. Other resonances contribute very weakly. Of course, our results are quite dependent on the CCs of various vertices, which are somewhat uncertain. Nevertheless, the relative cross sections shown in this figure are robust. First of all these CCs provide a good description of the total as well a differential cross sections of the elementary Ξ^- production reaction. Secondly there is very little scope for increasing further the individual contributions of the Λ and Σ

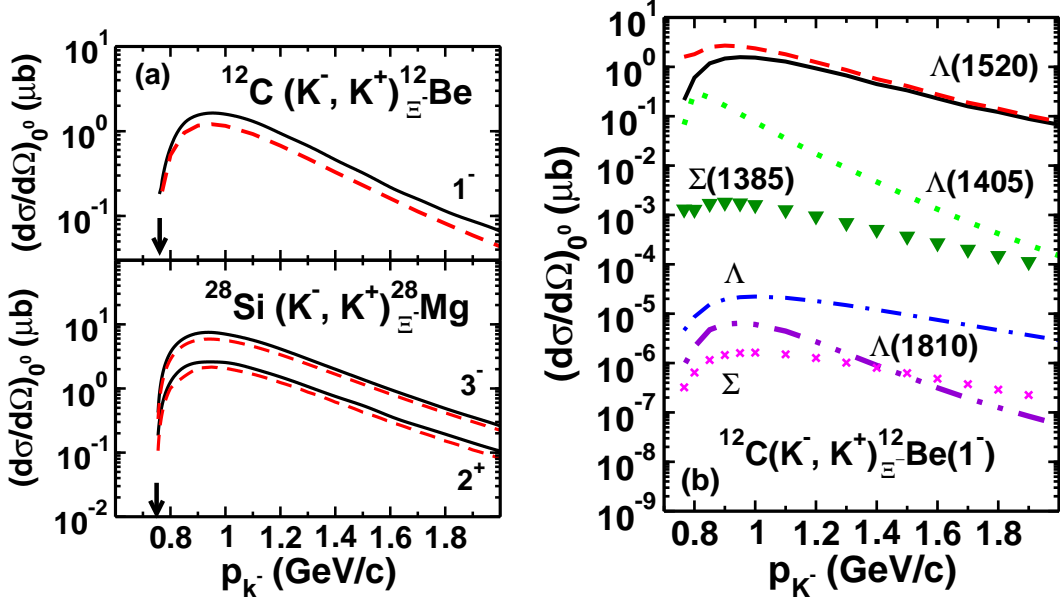


FIG. 4: (color online) (a) Calculated differential cross section at 0° as a function of K^- beam momentum for $^{12}\text{C}(K^-, K^+)^{12}_{\Xi^-}\text{Be}$ reaction with the configuration $[(1p_{3/2})_p^{-1}, (1s_{1/2})_{\Xi^-}]1^-$ and $^{28}\text{Si}(K^-, K^+)^{28}_{\Xi^-}\text{Mg}$ reactions with configurations $[(1d_{5/2})_p^{-1}, (1s_{1/2})_{\Xi^-}]2^+$, and $[(1d_{5/2})_p^{-1}, (1p_{3/2})_{\Xi^-}]3^-$ as indicated in each case by the final angular momentum state. The solid and dashed lines show the results obtained with QMC and phenomenological Ξ^- bound state spinors. Arrows show the threshold of the two reactions. (b) Contributions of individual resonance intermediate states as indicated near each line, to the zero angle differential cross section as function of K^- beam momentum for the $^{12}\text{C}(K^-, K^+)^{12}_{\Xi^-}\text{Be}(1^-)$ reaction as a function of K^- beam momentum. Their coherent sum is shown by the solid line.

intermediate states, because the CCs of the corresponding vertices used by us are already larger than their upper limits suggested in the literature. Furthermore, the contributions of other resonances are too weak and even have the wrong p_{K^-} dependence. Therefore, the final results are unlikely to be affected too much by the known uncertainties in the corresponding CCs.

In summary, in this paper the cascade hypernuclear production reactions $^{12}\text{C}(K^-, K^+)^{12}_{\Xi^-}\text{Be}$, and $^{28}\text{Si}(K^-, K^+)^{28}_{\Xi^-}\text{Mg}$ have been studied within an effective Lagrangian model, using the proton hole and Ξ^- bound state spinors derived from the latest quark-meson coupling model. This is for the first time that the quark degrees of freedom have been explicitly invoked in the description of such reactions. We have considered the

excitation of altogether six Λ and Σ hyperon resonance intermediate states in the initial collision of the K^- meson with a target proton. These states subsequently propagate and decay into a Ξ^- hyperon and a K^+ meson. The hyperon gets captured in one of the nuclear orbits, while the meson goes out. We constrain the coupling constants at the resonance vertices by describing both the total and the differential cross sections of the elementary $p(K^+, K^-)\Xi^-$ reaction within a similar model.

We have also performed calculations with the spinors obtained by solving the Dirac equation with vector and scalar potential fields having Woods-Saxon shapes (the phenomenological model). Their depths are fitted to the binding energies of the respective states (QMC model values for the Ξ^- particle states and experimental values for the proton hole states) for a given set of geometry parameters which are taken to be the same for the two fields. While for $^{12}_{\Xi^-}\text{-Be}$ hypernucleus the shapes of the QMC fields are similar to those of the phenomenological model, the two differ considerably in the case of $^{28}_{\Xi^-}\text{-Mg}$. For the cases studied in this paper, the hypernuclear production cross sections calculated with the QMC Ξ^- spinors are about 10-20% higher in magnitude to those obtained within the phenomenological model. The distortion effects are included by introducing reduction factors to the cross sections taken from the previous studies of this reaction.

The zero degree differential cross sections for the Ξ^- hypernuclear production reactions on the two targets considered here, have peaks around the beam momentum of 1.0 GeV/c within both the QMC and the phenomenological models. This peak momentum is above the corresponding production threshold by almost the same amount as the position of the maximum in the elementary cross section lies away from its respective threshold. The peak cross sections are in excess of 1 μb . Furthermore, the total hypernuclear production cross sections are dominated by the contributions from the $\Lambda(1520)$ (D_{03}) resonance intermediate state which is similar to the case of the elementary Ξ^- production reaction. Other resonances make noticeable contributions only at beam momenta close to the production threshold of the reaction. It is desirable to perform measurements for the differential cross sections of the elementary Ξ^- production reaction in a wide beam momentum range.

This work was supported by the University of Adelaide and the Australian Research Council through grant FL0992247(AWT).

Bibliography

- [1] J. Schaffner-Bielich, Nucl. Phys. **A 804** (2008) 309; *ibid.* Nucl. Phys. **A 835** (2010) 279c.
- [2] J. M. Lattimer and M. Prakash, Science **304** (2004) 536.
- [3] J. Adams *et al.*, Phys. Rev. Lett. **98** (2007) 062301; J. H. Chen, Nucl. Phys. **835** (2010) 117c.
- [4] K. Aamodt *et al.* (ALICE collaboration), Phys. Rev. Lett. **106** (2011) 032301.
- [5] CBM Physics Book, Springer, 2011; <http://www.gsi.de/fair/experiment/CBM/PhysicsBook.html>
- [6] R. L. Jaffe, Phys. Rev. Lett. **38** (1977) 195
- [7] P. J. Mulders and A. W. Thomas, J. Phys. **G 9** (1983) 1159.
- [8] S. R. Beane *et al.*, Phys. Rev. Lett. **106** (2011) 162001; T. Inoue *et al.*, *ibid.* **106** (2011) 162002; P. E. Shanahan, A. W. Thomas, and R. D. Young, *ibid.* (2011) 092004.
- [9] A. T. M. Aerts and C. B. Dover, Phys. Rev. Lett. **49** (1982) 1752.
- [10] A. T. M. Aerts and C. B. Dover, Phys. Rev. **D 28** (1983) 450.
- [11] T. Iijima *et al.*, Nucl. Phys. **A 546** (1992) 588.
- [12] T. Fukuda *et al.*, Phys. Rev. **C 58** (1998) 1306.
- [13] P. Khaustov *et al.*, Phys. Rev. **C 61** (2000) 054603.
- [14] D. H. Wilkinson *et al.*, Phys. Rev. Lett. **3** (1959) 397; A. Bechdolf *et al.*, Phys. Lett. **B26** (1968) 174.
- [15] T. Nagai *et al.*, JPARC proposal E05, http://j-parc.jp/NuclPart/Proposal_e.html.
- [16] C. B. Dover and A. Gal, Ann. Phys. (NY) **146** (1983) 309.
- [17] G. M. Pjerrou *et al.*, Phys. Rev. Lett. **9**, 114 (1962); J. Peter Berg *et al.*, Phys. Rev. **147**, 945 (1966); D. W. Merrill, and J. Button-Shafer, *ibid.* **167**, 1202 (1968); J. R. Carlson *et al.*, Phys. Rev. **D 7**, 2533 (1973); G. Burgun *et al.*, Nucl. Phys. **B8**, 447 (1968); E. Briefel *et al.*, Phys. Rev. **D 16**, 2706 (1977).
- [18] P. M. Dauber *et al.*, Phys. Rev. **179**, 1262 (1969).
- [19] V. Flaminio *et al.* CERN-HERA Report No. 83-02, 1983.
- [20] R. Shyam, O. Scholten and A. W. Thomas, Phys. Rev. **C 84** (2011) 042201(R).
- [21] Y. Yamamoto, T. Motoba, T. Fukuda, M. Takahashi and K. Ikeda, Progr. Theo. Phys. Suppl. **117** (1994) 281.
- [22] K. Ikeda, T. Fukuda, T. Motoba, M. Takahashi and Y. Yamamoto, Progr. Theo. Phys. **91** (1994) 747.

- [23] S. Tadokoro, H. Kobayashi, and Y. Akaishi, Phys. Rev. C **51** (1995) 2656.
- [24] T. Harada, Y. Hirabayashi and A. Umeya, Phys. Lett. **B 690** (2010) 363.
- [25] R. Shyam, H. Lenske and U. Mosel, Phys. Rev. C **69** (2004) 065205; *ibid.*, Nucl. Phys. **A764** (2006) 313; S. Bender, R. Shyam and H. Lenske, Nucl. Phys. **A 839** (2010) 51.
- [26] R. Shyam, H. Lenske and U. Mosel, Phys. Rev. C **77** (2008) 052201(R).
- [27] R. Shyam, K. Tsushima and A. W. Thomas, Phys. Lett. **B676** (2009) 51.
- [28] P. A. M. Guichon, Phys. Lett. **B200** (1988) 235; P. A. M. Guichon, K. Saito, E. N. Rodionov, and A. W. Thomas, Nucl. Phys. **A601** (1996) 349; P. A. M. Guichon, H. H. Matevosyan, N. Sandulescu, A. W. Thomas, Nucl. Phys. **A772** (2006) 1; K. Saito and A. W. Thomas, Phys. Rev. C **51** (1995) 2757.
- [29] B. D. Serot and J. D. Walecka, Adv. Nucl. Phys. **16** (1986) 1; *ibid.*, Int. J. Mod. Phys. **E 6** (1997) 515.
- [30] K. Saito, K. Tsushima and A. W. Thomas, Nucl. Phys. **A609** (1996) 339.
- [31] K. Tsushima, D. H. Lu, A. W. Thomas, and K. Saito, Phys. Lett. **B443** (1998) 26.
- [32] K. Tsushima, K. Saito, J. Haidenbauer and A. W. Thomas, Nucl. Phys. **A630** (1998) 691.
- [33] K. Tsushima, D. H. Lu, A. W. Thomas, K. Saito R. H. Landau, Phys. Rev. C **59** (1999) 2824; S. D. Bass and A. W. Thomas, Phys. Lett. **B634** (2006) 368.
- [34] K. Saito, K. Tsushima and A. W. Thomas, Prog. Part. Nucl. Phys. **58** (2007) 1.
- [35] J. Rikovska-Stone, P. A. M. Guichon, H. H. Matevosyan and A. W. Thomas, Nucl. Phys. **A792** (2007) 341.
- [36] P. A. M. Guichon, A. W. Thomas, and K. Tsushima, Nucl. Phys. **A 814** (2008) 66.
- [37] C. Bennhold and L. E. Wright, Phys. Rev. C **39** (1989) 927; *ibid.*, Phys. Lett. **B191** (1987) 11.
- [38] R. Shyam, Phys. Rev. C **60** (1999) 055213.